



Deposited via The University of Sheffield.

White Rose Research Online URL for this paper:

<https://eprints.whiterose.ac.uk/id/eprint/133555/>

Version: Accepted Version

Article:

Zheng, L., Ji, S. and Zhang, Y. (2018) Lifted and reattached behaviour of laminar premixed flame under external acoustic excitation. *Experimental Thermal and Fluid Science*, 98. pp. 683-692. ISSN: 0894-1777

<https://doi.org/10.1016/j.expthermflusci.2018.07.013>

Article available under the terms of the CC-BY-NC-ND licence
(<https://creativecommons.org/licenses/by-nc-nd/4.0/>).

Reuse

This article is distributed under the terms of the Creative Commons Attribution-NonCommercial-NoDerivs (CC BY-NC-ND) licence. This licence only allows you to download this work and share it with others as long as you credit the authors, but you can't change the article in any way or use it commercially. More information and the full terms of the licence here: <https://creativecommons.org/licenses/>

Takedown

If you consider content in White Rose Research Online to be in breach of UK law, please notify us by emailing eprints@whiterose.ac.uk including the URL of the record and the reason for the withdrawal request.

Lifted and reattached behaviour of laminar Premixed flame under external acoustic excitation

Lukai Zheng^{a*}, Shuaida Ji^b, Yang Zhang^b

^a Nanjing Institute of Technology, Nanjing 211167, China

^b University of Sheffield, Sheffield, S20 1AH, United Kingdom

Abstract

The flame chemiluminescent emission fluctuations and the vortex structure of the lifted jet flame under acoustic excitation were studied in this investigation. By employing high-speed visualization and DFCD (Digital Flame Colour Discrimination) image processing method, the fluctuation of the instantaneous mixture fraction has been found highly correlated with the lifted height variations. It has been observed that during the flame drifting to downstream, there is no obvious shifting on the mixture fraction. However, when the flame travels back to upstream, the fuel mixture has been evidently diluted. In addition, the stabilisation mechanism can be further explained by analysing the velocity fluctuation of the vortices in the shear layer via PIV. Measurements show that, the turbulent stretching at the shear layer generated by the excitation leading to the flame lift-off. on the other hand, the Kelvin-Helmholtz vortices in the unburn part play a key role in preventing flame lift-off. But, the excessive external acoustic excitation leads to blow-off due to over dilution and increased lifted height.

Keyword: *Acoustic excitation, Premixed flame, Flame lift-off, Kelvin-Helmholtz vortices.*

* Corresponding author E-mail: lukaizheng7@gmail.com (Lukai Zheng); yz100@sheffield.ac.uk (Yang Zhang)

21 **1 Introduction**

22 In most industrial applications, jet flame lifted off is always been regarded as the most
23 undesirable instability problem, as it's unstable and easy to blow-off abruptly. Hence, the stabilization
24 and extinction mechanism have been widely investigated numerically and experimentally.

25 A non-premixed jet flame has a tendency to lift off from the burner nozzle position when the
26 jet velocity of the flame is over a critical value of U_c [1]. With the increasing of the jet velocity, the
27 lifted height will increase and when it's beyond certain critical height and the flame will be blown off
28 [2]. Therefore, the stability of the lifted flame is an important parameter for basic combustor design.
29 Scholefield and Garside's theory [3] claimed that the transition to turbulence is a prerequisite for the
30 lifted diffusion flame stabilization and the flame anchors at a point where the flow is turbulent.
31 Gollahalli [4] argued that the flame will tend to stable at the position where the local flow velocity
32 balance the normal flame propagation velocity. Navarro-Martinez and Kronenburg [5] have
33 demonstrated that the excessive turbulent stretching at the nozzle leads to the lift-off and they also
34 claimed that auto-ignition can be used to promote the flame stabilization mechanism. Recently the
35 observation from Kiran and Mishra's [2] visual experiment proved the flame lift-off height varies
36 linearly with jet exit velocity. They presented a semi-empirical correlation between the normalized lift-
37 off height to the nozzle exit diameter.

$$38 \quad \frac{H_L}{D_f} = 1.8 \times 10^{-3} \frac{U_f}{D_f}$$

39 H_L : lift-off height

40 D_f : diameter of the fuel tube

41 U_f : fuel jet velocity

42 In addition to the velocity effect, The stoichiometric burning on the physical mechanism
43 blowout has been investigated by Broadwell et al. [6] and Pitts [7]. According to their study on
44 diffusion flame, the fresh air entrained by the vortices structure cools down and over dilutes the flame
45 jet, which leads to the flame extinction.

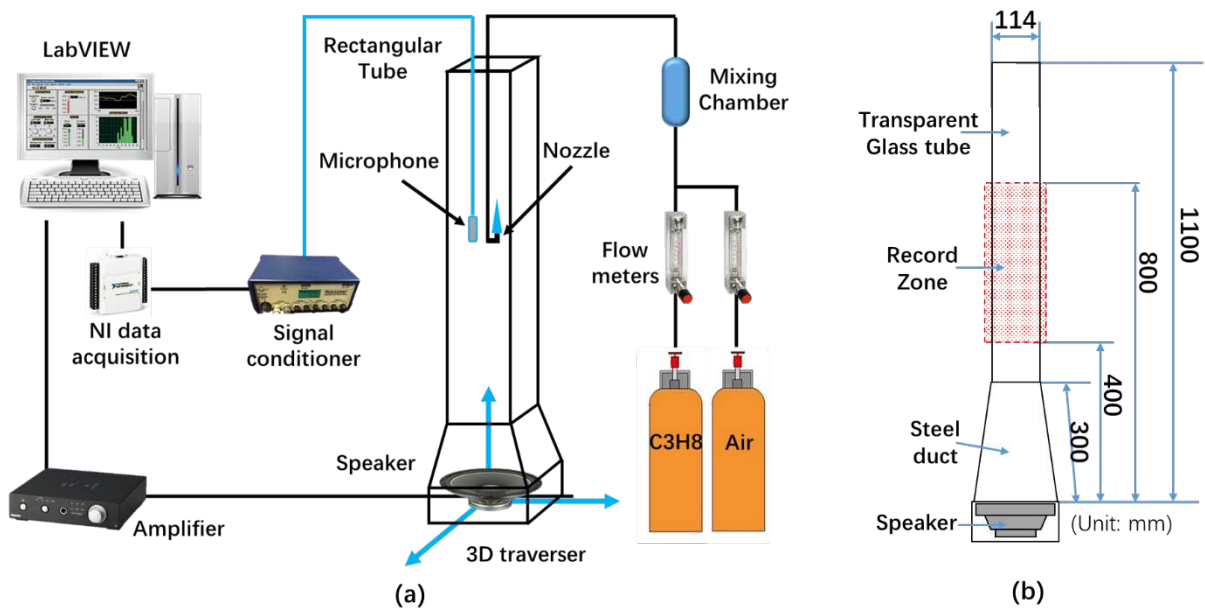
46 For a lifted flame, it has been shown by many researchers that, the rolling-up processes of
47 vortices structure generated by the bluff body or acoustic perturbation will prevent the lifted flame
48 from propagating downstream [8–12]. Flame response to specific external excitation in the terms of
49 frequency and amplitude was studied theoretically and experimentally by Demare and Baillet [13].
50 They concluded that secondary vortices are sufficiently powerful to make the flame propagate
51 oppositely. The flame lifting and reattaching characteristics and hysteresis zone where the flame
52 anchoring may occur has been noticed by Gollahall in 1986. [4] The study of diffusion flame stability
53 mechanisms in the hysteresis region by acoustically exciting the unburned components has been
54 investigated by Lin et al.[14] and [9], The most significant effect was found when the acoustic
55 frequency matched the fundamental frequency of the vortex. Chao et al. have demonstrated that, the
56 acoustic excitation at certain frequencies could extend the blowout limit by more than 25% [9].
57 Moreover, the stability method of acoustic excitation on lifted flame also has been proved to be feasible
58 for soot suppression and emission control[15–17].

59 On the other hand, Kim et al. [18] and Kartheekeyan et al. [19] have observed that, for
60 premixed flame, the flow oscillation affects the local strain rate at the shear layers, which contributes
61 to the fluctuation of heat release rate and mixing rate. Additionally, the unsteady vortical structure
62 pass by can stretch and quench the flame[20]. However, the variation of the local fuel to air ration by
63 these vortices cannot be ignored as it will be demonstrated in this study. Chen and Zhang has
64 experimentally investigated the nonlinear coupling characteristics on different equivalence ratios of
65 propane/air flame [21]. It has showed the existence of complex nonlinear frequency components
66 created by the coupling of buoyance driven instability and the acoustic excitation.

67 While the acoustic excitation has been widely investigated from two aspects: the acoustic
68 stabilization mechanism for diffusion flame and the flame shear layer dynamic experimentally [19,22–
69 26] or numerically [27] for premixed flame. There is lack of the knowledge on the transient dynamics
70 of the lifted and reattached phenomenon for the premixed flame. The present work investigates a
71 conical laminar premixed flame in a rectangular tube excited by acoustic wave. A comprehensive
72 analysis on the premixed flame periodically lifted and reattached phenomenon induced by external

73 acoustic excitation with the combination of diagnostic methods, colour imaging [28], schlieren and
 74 PIV methods. The periodical mechanism has been addressed from two aspects: the velocity field of
 75 the vorticity at the shear layers and premixed flame stoichiometry burning propagation preference. The
 76 Digital Flame Colour Discrimination (DFCD) technique is a unique method to analysis equivalence
 77 ratio fluctuation and the transient flame shear layer dynamics. It provides a more intuitive evaluation
 78 on the fuel concentration distribution. Combined with the Kelvin-Helmholtz vortex structure observed
 79 from the schlieren method, the results provide a good explanation for the flame reattachment progress.
 80 The oscillatory behaviour of laminar flame dynamic structure and lifted height are experimentally
 81 investigated with time resolved contour line detection method.

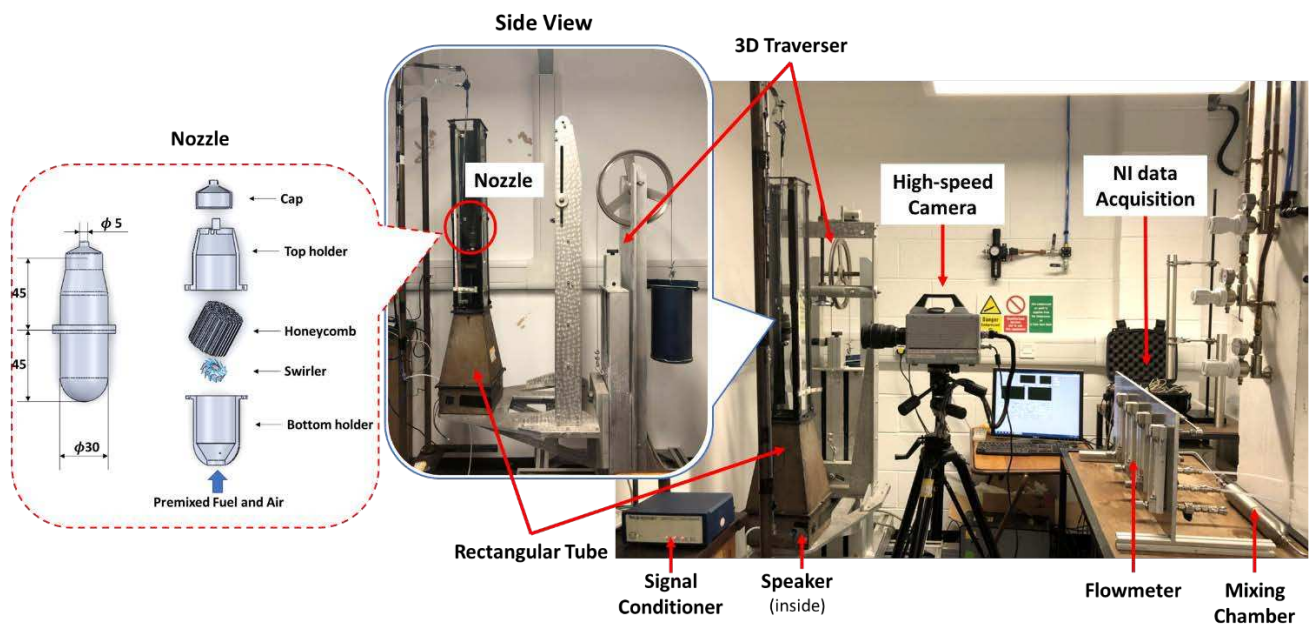
82 2 Experiment setup



83
 84 **Figure 1. (a) The experimental apparatus; (b) Schematic of the geometry of the square tube**
 85 **and loudspeaker**

86 The schematic of the experimental apparatus is shown in Figure 1 and the actual picture of the
 87 setup is shown Figure 2. The experimental setup mainly contains two systems: a burner system and an
 88 acoustic generating and sound acquisition system. In the burner system, the gaseous fuel and air are
 89 supplied from a propane cylinder and air compressor. The flow rate is controlled by a rotameter. The

90 fuel and air are connected with a mixing chamber to produce a premixed flame at the equivalence ratio
 91 of 1.4 (C_3H_8 0.12L/min; Air 2.046L/min). The nozzle position can be adjusted within the top end
 92 opened tube, which is made with four glass panels and braced by four steel brackets. The fuel nozzle
 93 is customized built, and the main dimensions are listed in the in Figure 2 the unit of mm. The shell of
 94 the nozzle can be separated into two parts, named top holder and bottom holder. These two parts are
 95 sealed properly when flame on. Inside of the shell, it mainly contains a swirler to stabilize the flame
 96 and a honeycomb to smooth the fuel flow.



97
 98 **Figure 2 Actual picture of the set-up**

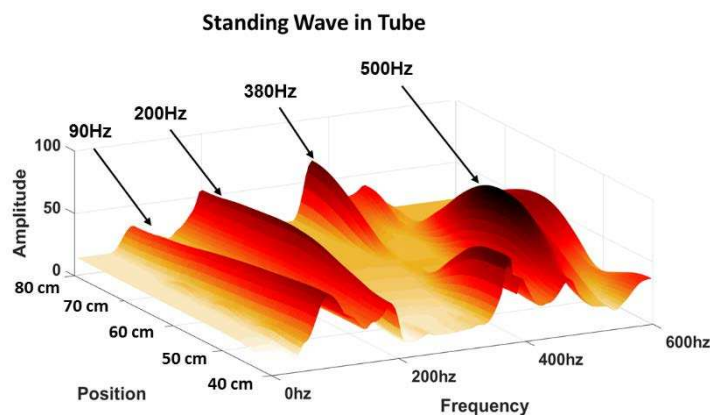
99 The dimensions of the tube are 1100 mm in length and 114 mm in width of the square. A large
 100 chamber is deliberately chosen so that the feedback mechanism from the flame itself can be minimised.
 101 The details geometry of the square tube is shown in Figure 1 (b). It consists the transparent top tube
 102 and steel pyramidal tube at the bottom. As the top end of the tube is open, to avoid the disturbance of
 103 the ventilation system in the lab, the nozzle position should keep a certain distance away from the top
 104 end. Considering the field of observation and the repeatability, the flame pattern and the sound pressure
 105 have been recorded within the range of the tube from 400 mm to 800 mm. The acoustic generator was
 106 placed at the bottom end of the tube and fixed on a computer controlled 3-D traverse system. The

107 frequency of the acoustic generating system was controlled by LabVIEW and the output voltage (V)
 108 of the amplifier was fixed at 3V. The reading of the sound pressure was collected by a microphone
 109 which is mounted at the nozzle and recorded by the National Instruments DAQ card. The measurement
 110 uncertainty is presented in Table 1.

111 **Table. 1 Experimental Uncertainty for Control Variables**

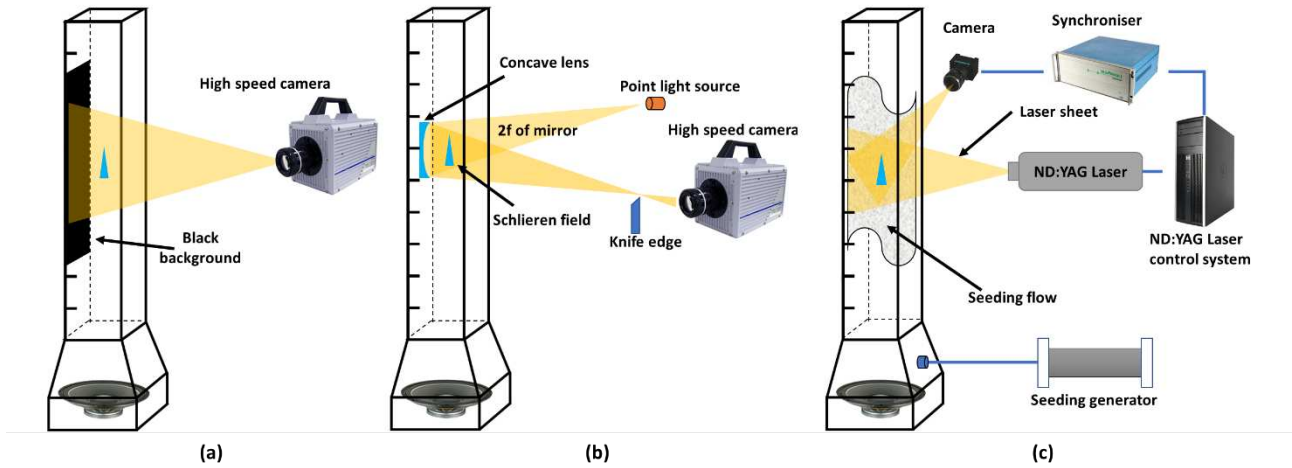
Measured Quantity	Measured Range	Total Measurement Uncertainty %
Fuel Flowmeter (L/min)	0 – 320	± 3 %
Air Flowmeter (L/min)	0 – 5	± 3 %
Microphone (Pa)	0 – 500	± 1 %
Amplifier (V)	0 – 5	± 1 %
3D Traverser (m)	0-1	± 2%

112 According the Previous research done by Chen [29], the four resonant frequencies in this duct are
 113 63.61Hz, 218.01Hz, 385.11Hz and 547.71Hz. These results are measured at the room temperature
 114 condition without the flame on. The standing wave in the duct can be affected by the temperature and
 115 the flame. Therefore, the experimental measurements of the acoustic responses were made along the
 116 length of the tube using a microphone with the flame on. The pressure value has been recorded at
 117 different position from 400mm to 800mm with 2 mm intervals through the whole tube and the
 118 measurement point was in the centre of the tube. The range of excitation frequency was from 20 Hz to
 119 600 Hz in increments of 5 Hz, with a voltage amplitude of 5 V. The experimental observation in Figure
 120 3 indicates that the first four modes of the present rig are 90 Hz, 200 Hz, 380 Hz, and 500 Hz.



121
 122 **Figure 3 Experimental measurement of pressure response to position and frequency with**
 123 **flame on**

124 The acoustic induced lifted-off behaviour is more evident under the high excitation frequency and
 125 high-pressure condition. Hence, the acoustic excitation frequencies of 380 Hz and 500 Hz were set as
 126 main frequencies for further investigation.



127

128 **Figure 4 (a) colour imaging recording setup; (b) Schlieren system setup; (C) PIV system**
 129 **setup**

130 The optical record setup consists of a Photron-SA4 high speed colour camera with Sigma zoom
 131 24-70mm lens and the computer control and recording system. Both of the colour and schlieren images
 132 were recorded by the high-speed camera at the full frame of 1024×1024 pixels. The colour image
 133 recording method is shown in Figure 4 (a). To avoid the background noise signals affecting the weak
 134 flame signal detection, the experiments were carried out in a dark room in addition to using black
 135 background behind the flame. To ensure the accuracy and generalization, 2000 images were recorded
 136 at a shutter speed of 2000 images per second at each condition. The images were analysed by MatLab.

137 A single mirror schlieren imaging system was applied to visualise the flow dynamics and vortex
 138 structure. With this configuration, vortices in the hysteresis region and the self-illuminated flame were
 139 both clearly shown in the schlieren images. The setup for schlieren system is shown in Figure 4 (b). It
 140 consists of a point light source and one $\lambda/10$ parabolic mirror with 75 mm diameter and 75 cm focal
 141 length. A knife edge is placed at the focal point, just in front of camera, to adjust the brightness and
 142 contrast.

143 The flow field is measured by a PIV system which consists of a laser sheet generator, a laser pulse

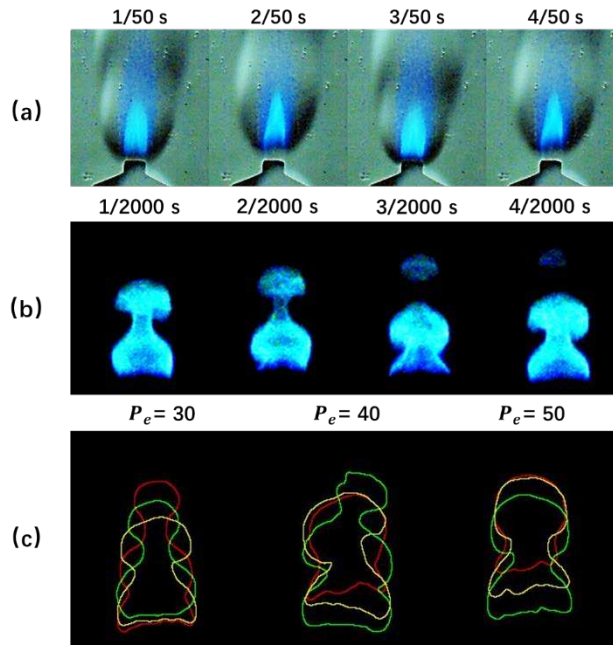
144 synchroniser, a seeding generator, a data acquisition system and data analysis software, shown in
145 Figure 4 (c). A double-pulse ND: YAG laser, operating at a wavelength of 532 nm, a pulse rate of 15
146 Hz and an energy per pulse of 190 mJ is used in this experiment and it is synchronized with a TSI
147 PowerviewTM Plus 4MP Camera used to capture particle images. The Laserpulse Synchroniser model
148 610035 from TSI is a timing control unit for the PIV applications. It automates control of the timing
149 between laser pulses, camera, camera interfaces and image acquisition. For PIV measurements, these
150 signals are controlled by the synchronizer via Insight 3G data acquisition, analysis and display software.
151 A solid particle generator and average 3 μm titanium dioxide TiO_2 seeding particles are used in this
152 experiment. These seeding particles are injected into the tube with the fuel and air together.

153 **3 Results and Analysis**

154 **3.1 Hysteresis Behaviour**

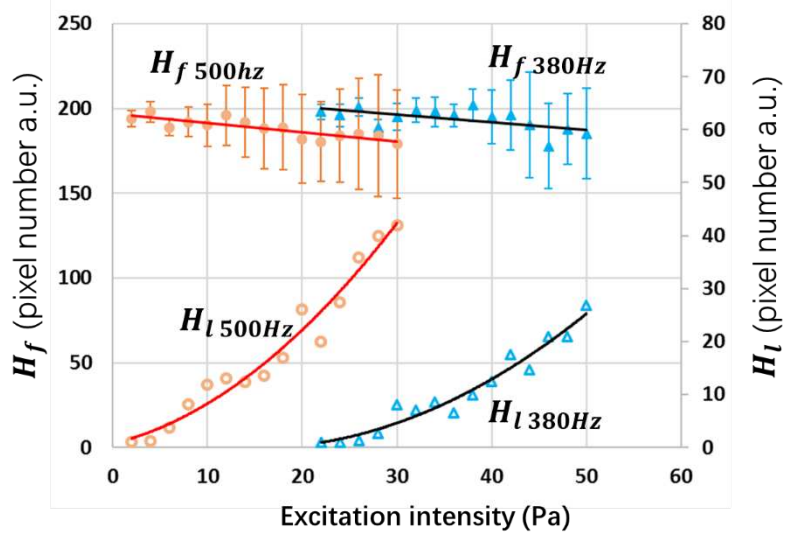
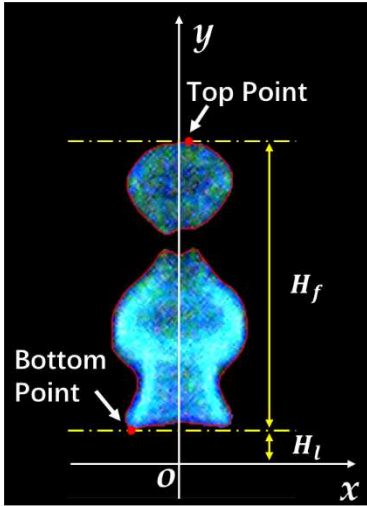
155 Figure 5 (a) presents the sequence of photographs from the single-mirror schlieren setting at an
156 excitation frequency of 380 Hz and forcing intensity of 40 Pa to show the hysteresis region and the
157 self-illuminated flame with shutter speed of 1/50 s at equal intervals. Under the strong excitation, the
158 periodical lifted-off and reattachment process of the premixed flame can be clearly observed in the
159 visible flame area. The motion is concurrent with the activity of the hot gas region.

160 To obtain a better observation of the flame periodically lifted behaviour, higher shutter speed
161 1/2000 s has been carried out for the visible flame imaging shown in Figure 5 (b). The samples of
162 series images in successive 4/2000 seconds display the visible flame front structure in transition of
163 lifted-off and reattachment. Under the acoustic forcing, the flame front exhibit severe deformation with
164 evident wrinkle fluctuation, separated flame bubbles and flame base lifted-up.



165
 166 **Figure 5 (a) The sequence of photographs from the single-mirror schlieren at a shutter**
 167 **speed of 1/50 s; (b) The samples of successive colour images in 4/2000 seconds; (c) Three**
 168 **sequential samples of the flame front contour lines with 1/2000 s interval**

169 A MatLab based contour detection algorithm has been employed to define the conical flame front
 170 and the extracted boundary lines are shown in Figure 5(c). The three sequential samples of the flame
 171 front contour lines with 1/2000 s interval from the 380 Hz frequency excitation case are drawn in each
 172 of the forcing pressure conditions, 30 Pa, 40 Pa and 50 Pa. The root segment of the front exhibits a
 173 noticeable position shifting in the vertical direction. The contour lines illustrate that the fluctuating
 174 amplitude of lifted height keeps growing with the increase of the perturbed pressure. In addition, the
 175 flame front exhibits an asymmetrically irregular geometry which is similar as what mentioned by
 176 Bourehla et al [30] and Gollahalli et al.[4]. These observations demonstrate that the lifted-off behaviour
 177 of premixed flame is sensitive to the external excitation. The formation of hysteresis and reattachment
 178 processes will be investigated and identified by its dominant flow characteristic in this experimental
 179 study.



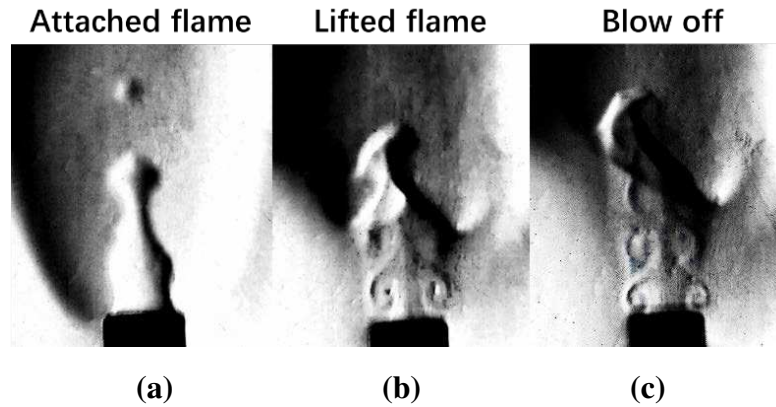
180
181

(a) (b)

182 **Figure 6 The variation of flame height H_f and lift-off height H_l of acoustically excited**
183 **flame**

184 The diagrammatic geometry of a 2D flame captured by the high-speed camera at a shutter speed
185 of 1/2000s with the selective colour enhancement technique is shown in Figure 6 (a). The red boundary
186 line of the flame presented the smoothing of the boundary gained through the application of the
187 interpolation points principle. The centre point (0, 0) of the coordinate system is located at the centre
188 of the nozzle exit. The flame length H_f is defined as the non-dimensional distance between the Top
189 Point and the Bottom Point calculated by the number of pixels in the y direction, shown Figure 6 (a).
190 The lift-off height H_l is defined by the distance in the y direction between the Bottom Point and the
191 nozzle exit. The value of the visible flame length H_f and the lift-off height H_l are the average of 500
192 selected images for each test case under forcing frequencies of 380 Hz and 500 Hz at different external
193 acoustic forcing intensity, shown in Figure 6 (b). The measurement of sound amplitude ranges from
194 the initial sign of lift-off to blow off point. Therefore, the amplitude ranges for the forcing frequencies
195 380 Hz and 500 Hz depended on their resistance of blow-off, 22—50 Pa and 2—30 Pa respectively.
196 The flame length H_f exhibits a descending trend for both frequency groups. The error bar presents
197 the standard deviation of flame lengths fluctuation amplitude. As can be obviously noticed from the
198 graph, the external sound pressure promotes the flame length fluctuation. This is mainly contributed
199 by the growing flame lifted height combined with the generation of separated flame bubbles. Moreover,

200 the growing rate of flame lifted height from 500 Hz frequency excitation is higher than that from 380
201 Hz frequency excitation, which indicated the premixed flame is prone to be disturbed and quenched
202 suddenly under high frequency acoustic perturbation condition. The observation is at variance with the
203 results of the non-premixed flame from Chen[31].



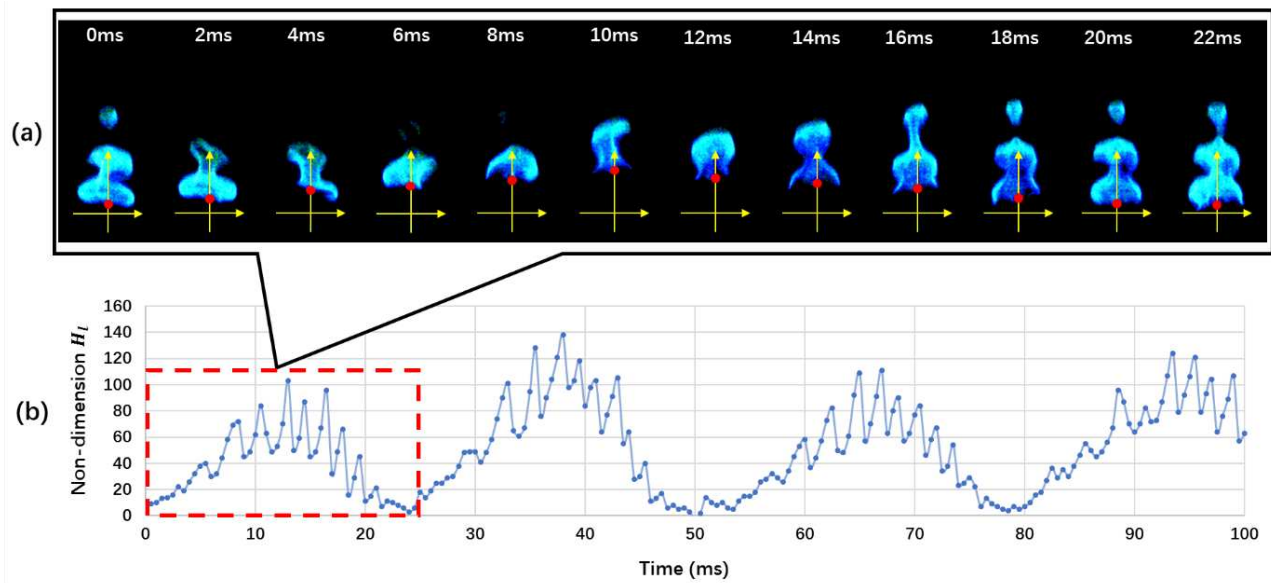
204
205
206 **Figure 7 Sample schlieren pictures for three perturbation conditions**

207 Figure 7 presents the sample schlieren picture at the salient feature point for each of three sound
208 perturbation conditions at 380 Hz, including attached flame (20 Pa), lifted flame (35 Pa) and blow off
209 (50 Pa). Although the vertical orientation of the knife edge is only sensitive to the radial density
210 gradients, the Kelvin-Helmholtz vortex structure become visible on the unburn jet shear layer near the
211 nozzle.

212 At the low sound amplitude level, the configuration of the flame front presents as a wavy
213 boundary before flame lifted. With the increase of the external perturbation, the waves overturn the
214 vicinity air and grow into billows in the unburning hysteresis region, which leads to the intermittent
215 flame holding. In the burning flame part, the convolutions structure become distorted and gradually
216 dissipated. Because the formation of the vortices structure is subsided as the presence of the flame
217 according to the studies by Gollahalli [4] and Chao [9]. Based on the observation of the massive
218 schlieren pictures, it is shown that the highest stabilized position is most probable at the top of the
219 second pairing of the coherent vortices. The stabilization mechanism of the Kelvin-Helmholtz vortex
220 structure will be further analysed in 3.3 and 3.4. With further increasing the sound pressure level causes
221 the server interference of the surrounding air and fuel. The excessive re-entrained cold fresh air from

222 the vortices cools down the hot products, which results in the reduction in heat release [32] and flame
 223 extinction eventually. During the blow-off procedure shown in Figure 7 (c), the organized stream-wise
 224 vortices pair gradually spread to larger-scale structure further downstream, which is in accordance with
 225 the observation by Demare et al.[11].

226 3.2 Nonlinear Coupling of Lifted Flame and Acoustic Wave



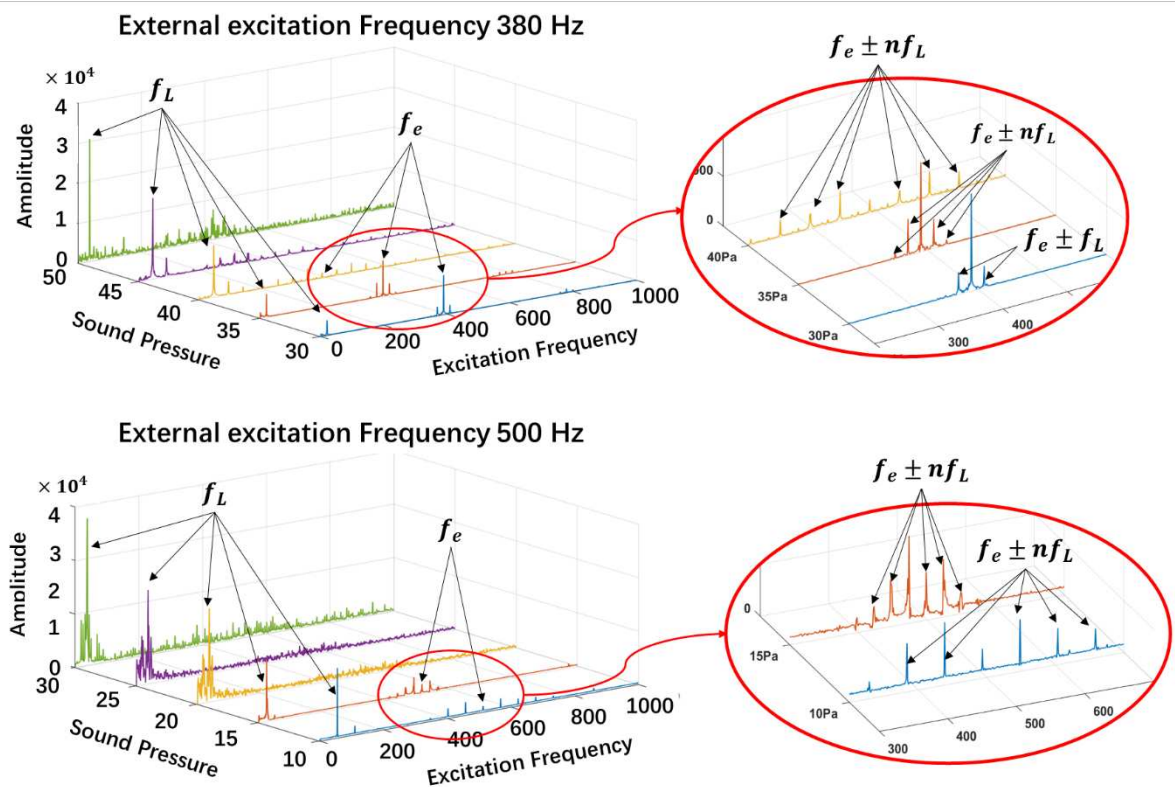
227

228 **Figure 8 (a) Colour images for circle process the attachment, lift-off and reattachment; (b)**
 229 **The trajectories of the flame lifted height**

230 Figure 8 (a) shows the sequence of the colour images for the flame in the transition circle
 231 process of attachment, lift-off and reattachment. The successive frames are at equal interval of 2ms.
 232 According to the coordinate system established in Figure 6, the trajectories of the visual flame lifted
 233 height, showed in Figure 8 (b), was recorded at 2000 fps in 100ms. As obviously shown in the graph,
 234 besides of the oscillations of lifting and reattachment, there was another high frequency oscillation
 235 throughout the time.

236 To determine the principle of the oscillations, FFT analysis was applied to the data of various
 237 acoustic intensities from the two frequency cases, shown in Figure 9. The FFT lines graph illustrates
 238 the dynamics of lifted height under various acoustic perturbations. The frequency components perform
 239 differently at different external excitation frequencies and intensities. Demare and Baillot [11] claimed

240 that the lifted-off height fluctuated randomly despite under the periodic forcing. However, as shown
 241 in the results, generally for all the cases, at particular excitation, the single peak of lift-off frequency
 242 f_L dominate the flame dynamic can always be detected in the range of 20 Hz to 40 Hz. That indicates,
 243 the fluctuation of the lifted height is not random, and it actually correlates to the formation conditions
 244 of the Kelvin-Helmholtz vortices and flame burning speed. The excitation frequencies f_e show more
 245 evident peaks under the tender acoustic forcing intensity. There is no nature flame flicking frequency
 246 can be detected, which indicates the buoyancy driving force doesn't have an effect on the flame lifted
 247 fluctuation at this low jet velocity ($Re= 557$).



248

249

Figure 9 The frequency of the lifted height for various acoustic excitation conditions

250

251

252

253

At the mild excitation amplitude in both cases of 380 Hz and 500 Hz, the sets of the fore and after
 peaks that accompany the dominated and harmonic frequencies $f_e \pm nf_L$ have been detected. The sets
 of accompanied fore and after peaks $f_e \pm nf_L$ are explained by nonlinear coupling theory, which has
 been reported by Wang [21] recently. The two frequencies components can be simplified into wave

254 signals, shown in below:

255
$$Y_{Excitation}(t) = x_e \sin(w_e t) \text{ and } Y_{Lifted}(t) = x_L \sin(w_L t);$$

256 The nonlinear coupling results in the creation of the frequency component as

257
$$Y_{coupling}(t) = k \sin(w_e t) \sin(w_L t);$$

258 This can then be broken down into the following equation:

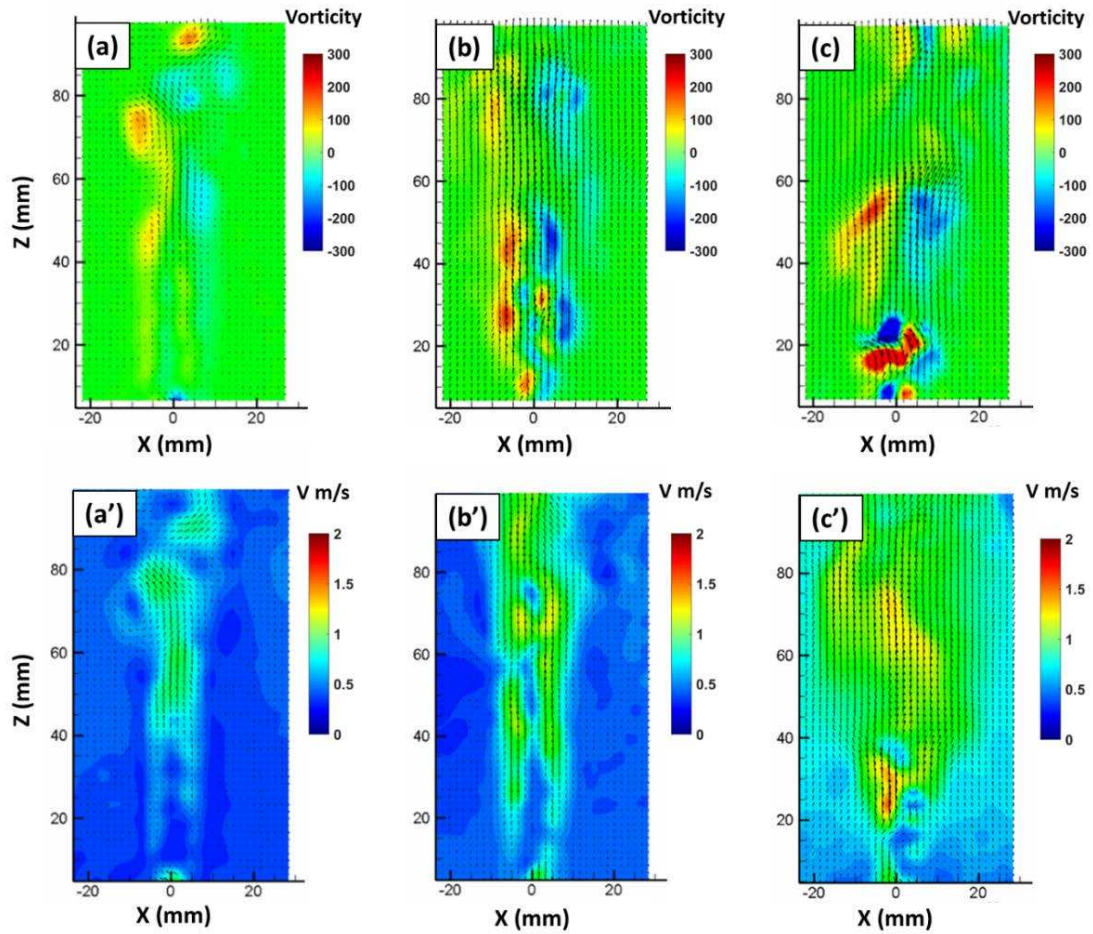
259
$$Y_{coupling}(t) = \frac{k[\cos(w_e - w_L) t] - [\cos(w_e + w_L) t]}{2}$$

260 Hence, this is the mainly explanation for the nonlinear coupling relationship of the $f_e \pm n f_L$.

261 The stabilization mechanism of the vortices has been reported by many researches [33,34]. The
262 researchers noticed that, for the lifted flame, at the hysteresis region, the vortices play an important
263 role for the flame stabilization and reattachment. Therefore, in the following paragraph the
264 phenomenon of acoustic induced lifted flame propagation procedure will be analysed mainly from two
265 aspects: the velocity and vorticity field with PIV measurement and the flame propagation preference
266 based on flame chemiluminescence detection.

267 **3.3 PIV measurements**

268 It's well-known that when the jet velocity U_{jet} larger than the burning velocity U_{burn} , the flame
269 detaches itself from the nozzle and stabilizes at the where $U_{jet} \approx U_{burn}$ in the downstream. The lifted
270 height is unstable, as the hysteresis zone is vulnerable to the external interference. PIV has been applied
271 to measure the velocity distribution of the jet with or without the vortices.



272

273

274

Figure 10. Velocity vectors and the vorticity contour maps of the instantaneous propane–air flame flow at the excitation frequency of 380Hz.

275

276

277

278

279

280

281

282

283

284

The contour maps of the velocity and vorticity for the premixed flame flow field under 380 Hz have been plotted in Figure 10. Three perturbation flame features induced by three sound intensities excitation levels have been investigated. Flame without excitation (a & a'), excited attached flame (b & b') and excited lifted flame (c and c') are shown from left to right in Figure 10. Under the external excitation condition, both of the fuel jet and the ambient air are disturbed by the acoustic wave. With the increase of the sound amplitude, the more obvious disturbance has been shown in the maps, especially for the area near the nozzle position at the coordination (0,0). From the plots of (a') and (b'), it's very interesting to notice that, before the flame lifted off, the velocity of the fuel jet at the upstream is smaller comparing with the ambient air and the relative velocity at the flame shear layer has been enlarged with the increase of the sound amplitude. Along the downstream, the air flow motion of the

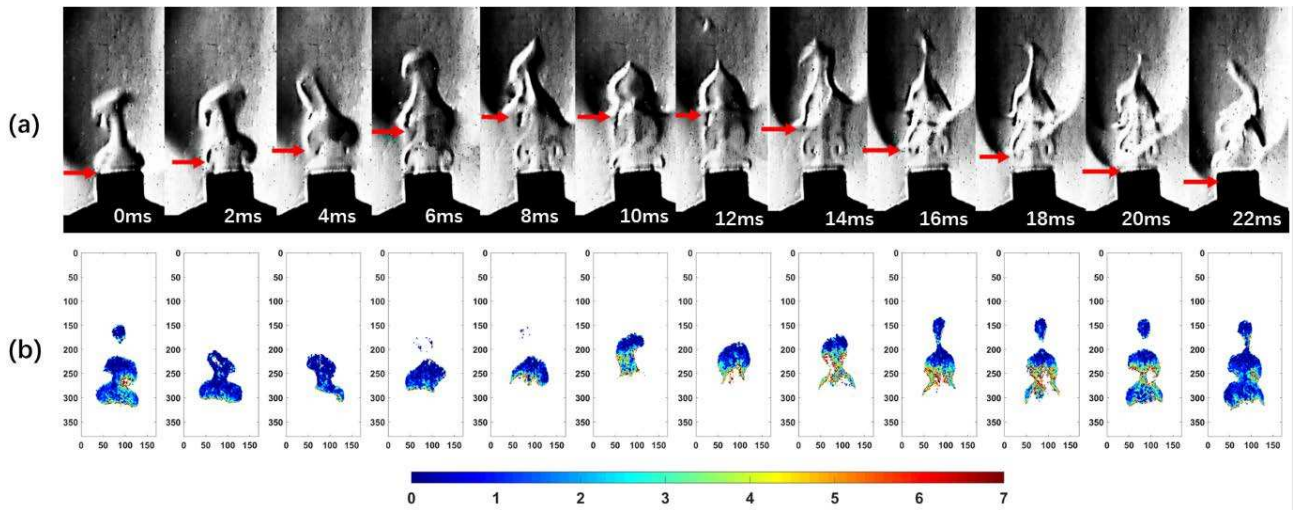
285 hot gas above the flame gradually further accelerates due to the buoyancy effect. Therefore, further
286 increasing the acoustic disturbance until the relative velocity at the shear layer reaches the critical
287 value U_c , and then the jet flame starts to lift off.

288 Contrary to the mild excited case, after the flame lifted-off, the relative velocity field condition
289 reversed, the velocity of unburned jet flow is much larger than that of the ambient air and the velocity
290 disparity results in the formation of Kelvin-Helmholtz vortices, which has been clear illustrated in (c).
291 There is much more intensive vorticity region concentrated above the nozzle. According to its
292 corresponding velocity map in (c'), at the Kelvin-Helmholtz rolling up region, there are obvious
293 downward velocity vectors in the flow pattern. This observation is matched with Chao's [9] and
294 Demare's [13] result. Chao et al. claimed that the local velocity of the vortex core region is higher than
295 the nature jet, but the outer edge of the layer and the mean velocity of the travelling wave has been
296 dramatically decreased. Therefore, the rolling-up vortices effectively prevent the lifted flame from
297 propagation upstream. Demare and Baillet presented velocity field of both the vertical and the
298 horizontal views. They found that the vortex radial velocity of the excited jet is nearly half of the
299 natural jet and the root-mean-square value is 25% lower [11]. Therefore, the Kelvin-Helmholtz ring
300 structure provides a suitable circumstance for the flame reattachment. Moreover, these vortex
301 structures not only minimise the velocity disparity at the shear layer, but also promote the further
302 mixing between the fuel and the ambient air. The mixture fraction will be further analysed by the
303 DFCD image processing method on the flame chemiluminescence.

304 **3.4 Flame Chemiluminescence**

305 The experimental data measured by Gu [35] proved that burning velocity for premixed flame
306 reaches its maximum value when the equivalence ratio is around 1. In addition, Walchshofer has
307 concluded that the lifted flame is stabilized close to the surface stoichiometric mixing conditions [36].
308 In another word, the premixed flame at equivalence ratio 1.4 preferably drifts towards the relatively
309 fuel leaner side. Many modelling works on premixed flame dynamics attempt to calculate the
310 equivalence ratio fluctuation response to imposed acoustic excitation [37–39]. The recent experimental

311 work by Kartheekyan and Chakravarthy [19] only presented a blurry configuration of the
 312 chemiluminescence images. The acoustic induced dilution behaviour can be quantitatively analysed
 313 with DFCD, which has been implemented in the present work for evaluating the distribution of fuel
 314 concentration. This method has been introduced in Huang's previous researches [28] and applied on
 315 both of gaseous [40] and liquid combustions [41].



316
 317 **Figure 11 (a) The schlieren images for flame and jet flow structure during the lifted and**
 318 **reattached process; (b) Instantaneous calculated CH^*/C_2^* ratio colour map**

319 the CH^*/C_2^* ratio has been proved to have monotonic relation with the equivalence ratio. It can
 320 be regarded as an indicator to reveal the fuel mixing fraction level, in which the fuel lean flame has
 321 higher CH^*/C_2^* ratio and high fuel concentration flame has lower CH^*/C_2^* ratio. Figure 11 (a) shows
 322 the sequence of the schlieren images for the flame lifted and reattached circle process with 2 ms
 323 intervals. The Kelvin-Helmholtz rolling-up structure can be clearly recognized in the unburnt jet region
 324 above the nozzle when the flame lifted. Figure 11 (b) presents the instantaneous colour map of the
 325 calculated CH^*/C_2^* ratio of the corresponding images. The ratio ranges from 0 to 7 and displays the
 326 colour from dark blue to red. During the flame propagating downstream, the flame area gradually
 327 decreases, but there is no evidence change in the fuel concentration and most of the flame area
 328 exhibited as dark blue. As soon as the flame lifted to the highest position, the reddish and yellowish
 329 colour gradually emerge at the bottom section, which indicates the vortex-up configuration enhances
 330 the mixing between the fuel and the surrounding air. During the falling period, the lifted flame

331 propagates upstream as a result of vortices induced local lower mixture fraction, which is consistent
332 with flame propagation preference. It's also worth noticing that, beside of the predominant distribution
333 zone of the reddish and yellowish points at the bottom region of the flame, it also occurs at the core of
334 the vortex. Therefore, based on all the discussion above, the upstream propagation behaviour of the
335 acoustic excited lifted flame could be explained by rolling-up vortices stabilization mechanism and
336 local mixing enhancement.

337 **4. Conclusion**

338 This study has presented a quantitative experimental observation on the acoustic excitation
339 induced lifted flame. The investigated lifted flame features include fluctuation of flame length and
340 lifted height, velocity field of the vortex structure, premixed flame fuel/air mixing ratio and
341 propagation behaviour. It has been observed that:

- 342 • The premixed flame is prone to be disturbed and can extinct suddenly under high frequency
343 acoustic perturbation condition. The fluctuating amplitude of lifted height keeps growing with
344 the increase of the forcing intensity. The flame blows off at 380 Hz/50 Pa and 500 Hz/30 Pa in
345 this case.
- 346 • The external forcing pressure promotes the flame height fluctuation due to the appearance of
347 the separated flame pocket. The growing rate of flame lifted height from 500 Hz frequency
348 excitation is higher than that from 380 Hz frequency excitation
- 349 • Kelvin-Helmholtz ring structure forms at the unburn jet boundary near the nozzle when flame
350 lifted, which can intermittently stabilize the flame. But the flame will blow off eventually under
351 the severe turbulence stretching due to the excessive re-entrainment of cold fresh air to cool
352 down the hot products and the flame fails to sustainable.
- 353 • Under the low forcing sound pressure, the non-constant value of lift-off frequency f_L has non-
354 linear coupling with the external excitation frequencies f_e , exhibited as $f_e \pm nf_L$. while as,

355 under the high forcing sound pressure, the vortices dominated the lifted height oscillation with
356 frequency f_L .

357 • Before flame lifted, relative velocity at the flame shear layer has been enlarged with the
358 increase of the sound amplitude; After the flame lifted, intensive vorticity region concentrated
359 at the Kelvin-Helmholtz rolling up region, which minimises the velocity disparity and provides
360 a suitable circumstance for the flame reattachment.

361 • During the flame propagating upstream, the CH^*/C_2^* ratio are significant increase at the
362 bottom area. Because, the moderate fresh air entrainment with Kelvin-Helmholtz vortices
363 structure dilutes the mixture fraction. The premixed flame burning speed and propagation
364 preference drag the flame back to the nozzle.

365

References

- 367 [1] D. Demare, F. Baillot, The role of secondary instabilities in the stabilization of a nonpremixed
368 lifted jet flame, *Phys. Fluids*. 13 (2001) 2662–2670. doi:10.1063/1.1386935.
- 369 [2] D.Y. Kiran, D.P. Mishra, Experimental studies of flame stability and emission characteristics of
370 simple LPG jet diffusion flame, *Fuel*. 86 (2007) 1545–1551. doi:10.1016/j.fuel.2006.10.027.
- 371 [3] D.A. Scholefield, J.E. Garside, The structure and stability of diffusion flames, in: *Symp.*
372 *Combust. Flame, Explos. Phenom.*, Elsevier, 1948: pp. 102–110.
- 373 [4] S.R. Gollahalli, Ö. Savaş, R.F. Huang, J.L. Rodriguez Azara, Structure of attached and lifted
374 gas jet flames in hysteresis region, *Symp. Combust.* 21 (1988) 1463–1471. doi:10.1016/S0082-
375 0784(88)80379-5.
- 376 [5] S. Navarro-Martinez, A. Kronenburg, Flame stabilization mechanisms in lifted flames, *Flow,*
377 *Turbul. Combust.* 87 (2011) 377–406.
- 378 [6] J.E. Broadwell, W.J.A. Dahm, M.G. Mungal, Blowout of turbulent diffusion flames, *Symp.*
379 *Combust.* 20 (1985) 303–310. doi:10.1016/S0082-0784(85)80515-4.
- 380 [7] W.M. Pitts, Assessment of theories for the behavior and blowout of lifted turbulent jet diffusion
381 flames, *Symp. Combust.* 22 (1989) 809–816. doi:10.1016/S0082-0784(89)80090-6.
- 382 [8] S. Chaudhuri, S. Kostka, M.W. Renfro, B.M. Cetegen, Blowoff dynamics of bluff body
383 stabilized turbulent premixed flames, *Combust. Flame*. 157 (2010) 790–802.
384 doi:10.1016/j.combustflame.2009.10.020.
- 385 [9] Y.-C. Chao, J. Ming-Shan, Behavior of the lifted jet flame under acoustic excitation, *Symp.*
386 *Combust.* 24 (1992) 333–340. doi:10.1016/S0082-0784(06)80044-5.
- 387 [10] F. Baillot, D. Demare, Physical Mechanisms of a Lifted NonPremixed Flame Stabilized in an
388 Acoustic Field, *Combust. Sci. Technol.* 174 (2002) 73–98. doi:10.1080/713713066.
- 389 [11] D. DEMARE, F. BAILLOT, Acoustic enhancement of combustion in lifted nonpremixed jet
390 flames, *Combust. Flame*. 139 (n.d.) 312–328.
391 <http://cat.inist.fr/?aModele=afficheN&cpsidt=16363812> (accessed February 23, 2017).
- 392 [12] J. Oh, Q.S. Khan, Y. Yoon, Acoustic excitation effect on NO_x reduction and flame stability in a
393 lifted non-premixed turbulent hydrogen jet with coaxial air, *Fuel*. 89 (2010) 1492–1498.
394 doi:10.1016/j.fuel.2009.10.001.
- 395 [13] D. Damare, F. Baillot, The role of secondary instabilities in the stabilization of a nonpremixed
396 lifted jet flame, *Phys. Fluids*. 13 (2001) 2662–2670. doi:10.1063/1.1386935.
- 397 [14] C.K. Lin, M.S. Jeng, Y.C. Chao, The stabilization mechanism of the lifted jet diffusion flame in
398 the hysteresis region, *Exp. Fluids Exp. Methods Their Appl. to Fluid Flow*. 14 (1993) 353–365.
399 doi:10.1007/BF00189494.

- 400 [15] M. Kim, Y. Choi, J. Oh, Y. Yoon, Flame-vortex interaction and mixing behaviors of turbulent
401 non-premixed jet flames under acoustic forcing, *Combust. Flame.* 156 (2009) 2252–2263.
402 doi:10.1016/j.combustflame.2009.08.004.
- 403 [16] J. Oh, Q.S. Khan, Y. Yoon, Nitrogen dilution effect on flame stability in a lifted non-premixed
404 turbulent hydrogen jet with coaxial air, *Fuel.* 89 (2010) 1492–1498.
405 doi:10.1016/j.fuel.2009.10.001.
- 406 [17] Y. Chao, D. Wu, C. Tsai, Effects of Acoustic Excitation on the Combustion and Pollution
407 Emission Characteristics of a Jet Flame, 0 (2000) 1–13.
- 408 [18] K.T. Kim, J.G. Lee, B.D. Quay, D.A. Santavicca, Response of partially premixed flames to
409 acoustic velocity and equivalence ratio perturbations, *Combust. Flame.* 157 (2010) 1731–1744.
410 doi:10.1016/j.combustflame.2010.04.006.
- 411 [19] S. Kartheekyan, S.R. Chakravarthy, An experimental investigation of an acoustically excited
412 laminar premixed flame, *Combust. Flame.* 146 (2006) 513–529.
413 doi:10.1016/j.combustflame.2006.04.014.
- 414 [20] J.S. Kistler, C.J. Sung, T.G. Kreut, C.K. Law, M. Nishioka, Extinction of counterflow diffusion
415 flames under velocity oscillations, in: *Symp. Combust.*, Elsevier, 1996: pp. 113–120.
- 416 [21] Q. Wang, H.W. Huang, H.J. Tang, M. Zhu, Y. Zhang, Nonlinear response of buoyant diffusion
417 flame under acoustic excitation, *Fuel.* 103 (2013) 364–372. doi:10.1016/j.fuel.2012.08.008.
- 418 [22] N. Karimi, M.J. Brear, S.H. Jin, J.P. Monty, Linear and non-linear forced response of a conical,
419 ducted, laminar premixed flame, *Combust. Flame.* 156 (2009) 2201–2212.
420 doi:10.1016/j.combustflame.2009.06.027.
- 421 [23] D.H. Shin, T. Lieuwen, Flame wrinkle destruction processes in harmonically forced, laminar
422 premixed flames, *Combust. Flame.* 159 (2012) 3312–3322.
423 doi:10.1016/j.combustflame.2012.06.015.
- 424 [24] A. Cuquel, D. Durox, T. Schuller, *Comptes Rendus Mecanique* Impact of flame base dynamics
425 on the non-linear frequency response of conical flames, *Comptes Rendus Mec.* 341 (2013) 171–
426 180. doi:10.1016/j.crme.2012.11.004.
- 427 [25] H.Y. Wang, C.K. Law, T. Lieuwen, Linear response of stretch-affected premixed flames to flow
428 oscillations, *Combust. Flame.* 156 (2009) 889–895. doi:10.1016/j.combustflame.2009.01.012.
- 429 [26] N. Karimi, Response of a conical, laminar premixed flame to low amplitude acoustic forcing -
430 A comparison between experiment and kinematic theories, *Energy.* 78 (2014) 490–500.
431 doi:10.1016/j.energy.2014.10.036.
- 432 [27] S. Schlimpert, M. Meinke, W. Schröder, Nonlinear analysis of an acoustically excited laminar
433 premixed flame, *Combust. Flame.* 163 (2016) 337–357.
434 doi:10.1016/j.combustflame.2015.09.035.
- 435 [28] H.W. Huang, Y. Zhang, Imaging based chemiluminescence characterisation of partially

- 436 premixed syngas flames through DFCD technique, *Int. J. Hydrogen Energy*. 38 (2013) 4839–
437 4847. doi:10.1016/j.ijhydene.2013.01.142.
- 438 [29] L. Chen, A theoretical and experimental study on flow characterisation in an acoustically excited
439 chamber, *Wave Motion*. 58 (2015) 68–76. doi:10.1016/j.wavemoti.2015.07.003.
- 440 [30] A. Bourehla, F. Baillot, Appearance and stability of a laminar conical premixed flame subjected
441 to an acoustic perturbation, *Combust. Flame*. 114 (1998) 303–318. doi:10.1016/S0010-
442 2180(97)00323-4.
- 443 [31] L.W. Chen, Y. Zhang, Experimental observation of the nonlinear coupling of flame flow and
444 acoustic wave, *Flow Meas. Instrum.* 46 (2015) 12–17. doi:10.1016/j.flowmeasinst.2015.09.001.
- 445 [32] D.M.H.-P. & K.C.S. E. GUTMARK, T. P. PARR, Stabilization of a Premixed Flame by Shear
446 Flow Excitation, *Combust. Sci. Technol.* 73 (1990) 521–535. doi:10.1080/00102209008951668.
- 447 [33] A. Onder, J. Meyers, Modification of vortex dynamics and transport properties of transitional
448 axisymmetric jets using zero-net-mass-flux actuation, *Phys. Fluids*. 26 (2014).
449 doi:10.1063/1.4890242.
- 450 [34] J. Lee, S.H. Won, S.H. Jin, S.H. Chung, Lifted flames in laminar jets of propane in coflow air,
451 *Combust. Flame*. 135 (2003) 449–462. doi:10.1016/S0010-2180(03)00182-2.
- 452 [35] X.J. Gu, M.Z. Haq, M. Lawes, R. Woolley, Laminar burning velocity and Markstein lengths of
453 methane–air mixtures, *Combust. Flame*. 121 (2000) 41–58. doi:10.1016/S0010-
454 2180(99)00142-X.
- 455 [36] C. Walchshofer, H. Steiner, Computational investigation of the stability of a lifted strongly
456 buoyant jet flame, *Combust. Flame*. 162 (2015) 613–627.
457 doi:10.1016/j.combustflame.2014.09.007.
- 458 [37] T. Lieuwen, Modeling Premixed Combustion-Acoustic Wave Interactions: A Review, *J. Propuls.*
459 *Power*. 19 (2003) 765–781. doi:10.2514/2.6193.
- 460 [38] J.H. Cho, T. Lieuwen, Laminar premixed flame response to equivalence ratio oscillations,
461 *Combust. Flame*. 140 (2005) 116–129. doi:10.1016/j.combustflame.2004.10.008.
- 462 [39] Shreekrishna, S. Hemchandra, T. Lieuwen, Premixed flame response to equivalence ratio
463 perturbations, *Combust. Theory Model.* 14 (2010) 681–714.
464 doi:10.1080/13647830.2010.502247.
- 465 [40] J. Yang, F.M.S. Mossa, H.W. Huang, Q. Wang, R. Woolley, Y. Zhang, ScienceDirect Oscillating
466 flames in open tubes, *Proc. Combust. Inst.* 35 (2015) 2075–2082.
467 doi:10.1016/j.proci.2014.07.052.
- 468 [41] L. Zheng, A. Faik, Y. Zhang, Flame colour analysis for the droplet combustion of water-in-diesel
469 emulsions, in: 12th Int. Conf. Heat Transf. Fluid Mech. Thermodyn., Malaga, Spain, 2016: pp.
470 212–217. <https://edas.info/web/hefat2016/titles.html#F>.

